Supporting Information

Layered $(NH_4)_2V_6O_{16}\cdot 1.5H_2O$ Nanobelts as a High-Performance Cathode for Aqueous Zinc-Ion Batteries

Xiao Wang,[a,d] Baojuan Xi,[a] Zhenyu Feng,[a] Weihua Chen,[b] Haibo Li,[c] Yuxi Jia,[d] Jinkui Feng,[d] Yitai Qian,[a] and Shenglin Xiong*[a]

[a] Key Laboratory of Colloid and Interface Chemistry, Ministry of Education, School of Chemistry and Chemical Engineering, and State Key Laboratory of Crystal Materials, Shandong University, Jinan 250100, P. R. China

[b] College of Chemistry and Molecular Engineering, Key Laboratory of Material Processing and Mold of Ministry of Education, Zhengzhou University, Zhengzhou 450001, P. R. China

[c] School of Chemistry and Chemical Engineering, Liaocheng University, Liaocheng, Shandong 252059, P. R. China

[d] Key Laboratory for Liquid-solid Structural Evolution & Processing of Materials (Ministry of Education), Shandong University, Jinan 250061, P. R. China

Correspondence and requests for materials should be addressed to S.L.X. (email: chexsl@sdu.edu.cn).

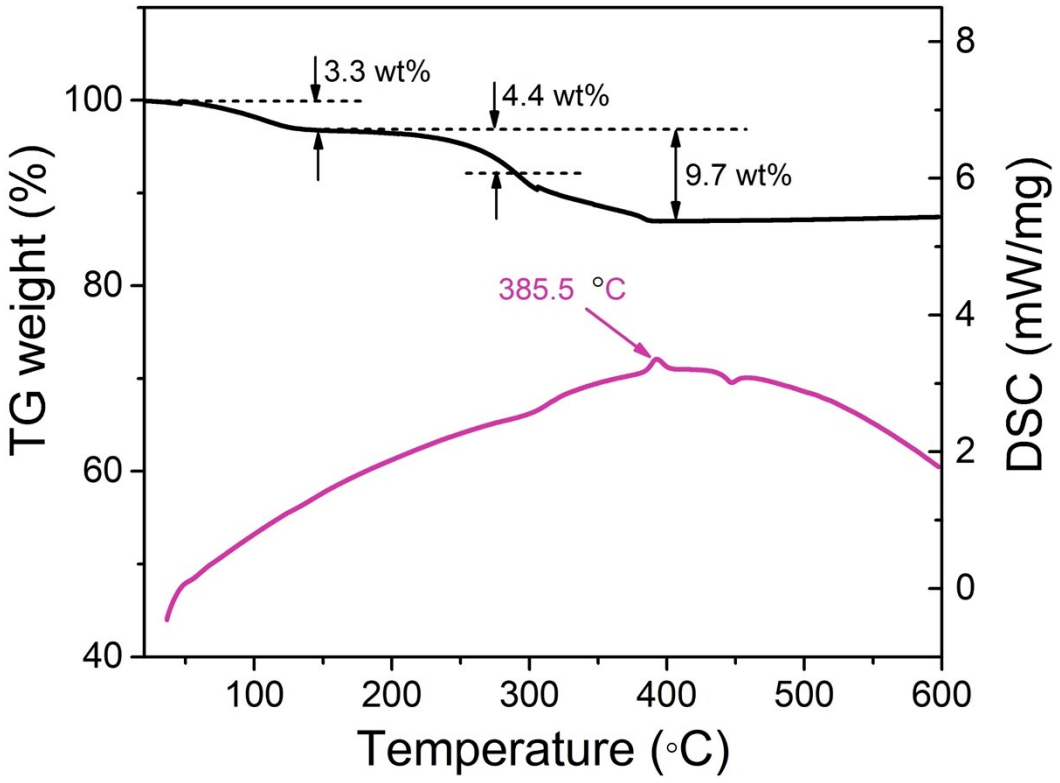

Figure S1. TG-DSC curves of the as-prepared H-NVO.

Note: As shown in Figure S1, the weight loss of about 3.3% before 150 ˚C belongs to the dehydration of physically absorbed water. After the temperature rises up to 280 ˚C, the additional weight loss of about 4.4% can be attributed to the desorption of crystal water in H-NVO. Based on this weight loss, it could be estimated that there are 1.52 crystal water in each formula unit of H-NVO, close to the theoretical value 1.57, further evidencing the phase structure of H-NVO. When the temperature continuously rises up to 385.5 ˚C, the phase transition temperature as shown from the DSC curve, the framework of H-NVO starts to collapse accompanied with the release of NH_3 due to the decomposition of the NH_4^+ and V_3O_8 group. Finally, the pure V_2O_5 was obtained, as evidenced in the XRD patterns shown in Figure S2.

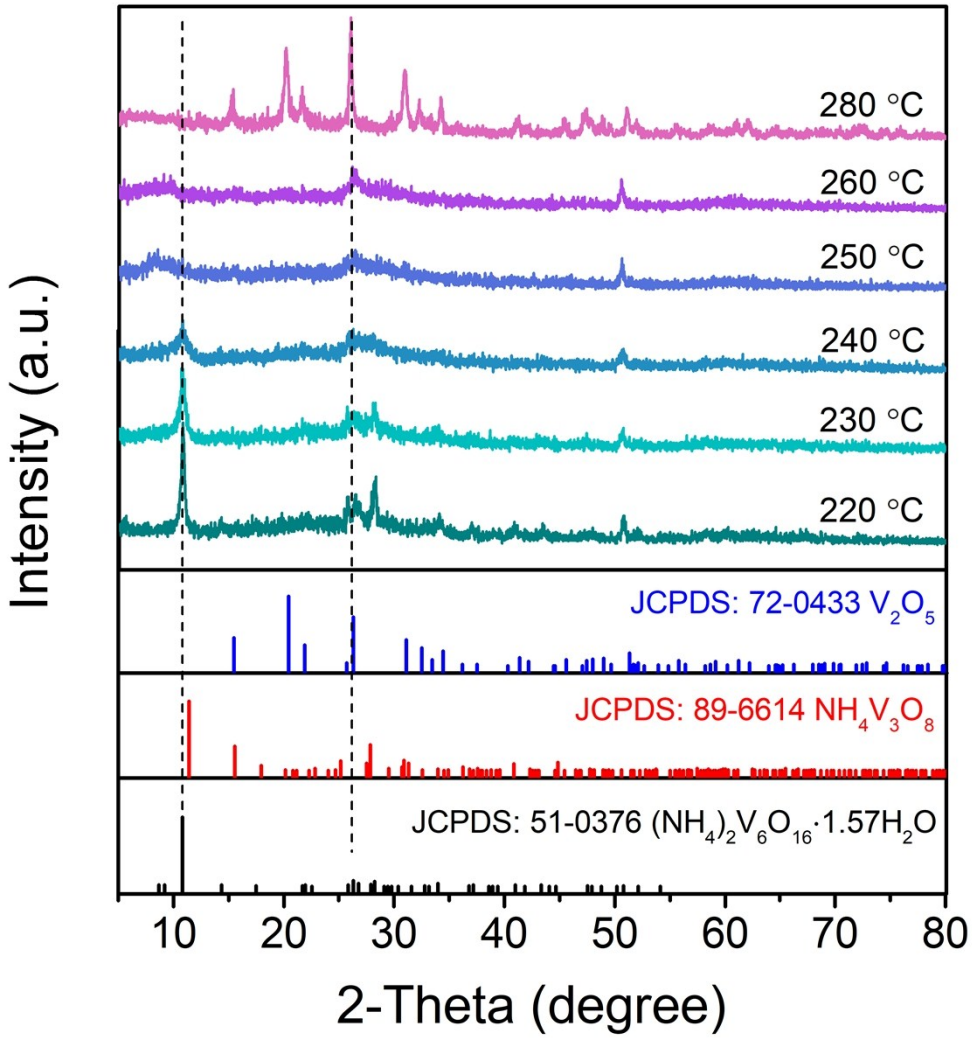

Figure S2. Power XRD patterns of the as-prepared H-NVO after the heat treatment at varied temperatures for 3 h in flowing argon atmosphere.

Note: As shown in Figure S2, the $(NH_4)_2V_6O_{16}\cdot 1.5H_2O$ phase could be maintained when heat-treated at 220-240 C. However, the intensities of the (002) peak located at 10.8º and the (112) peak located at 28.2º decreased with the elevated temperature, corresponding to the decrease of crystallinity. When heat-treated at 250 and 260 C, these two characteristic peaks disappeared accompanied by the appearance of a new characteristic peak located at 26.2º, which could be ascribed to the (101) lattice plane of V_2O_5. Finally, when heat-treated at 280 C, the pure V_2O_5 phase was obtained.

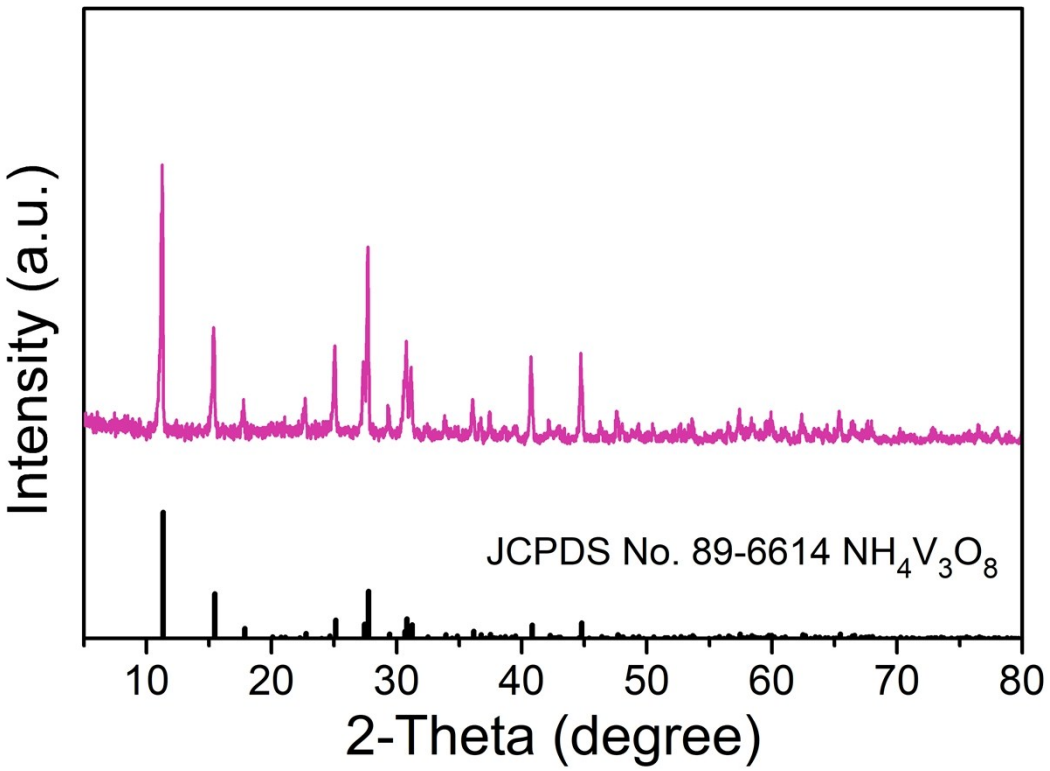

Figure S3. Power XRD patterns of the as-prepared NVO.

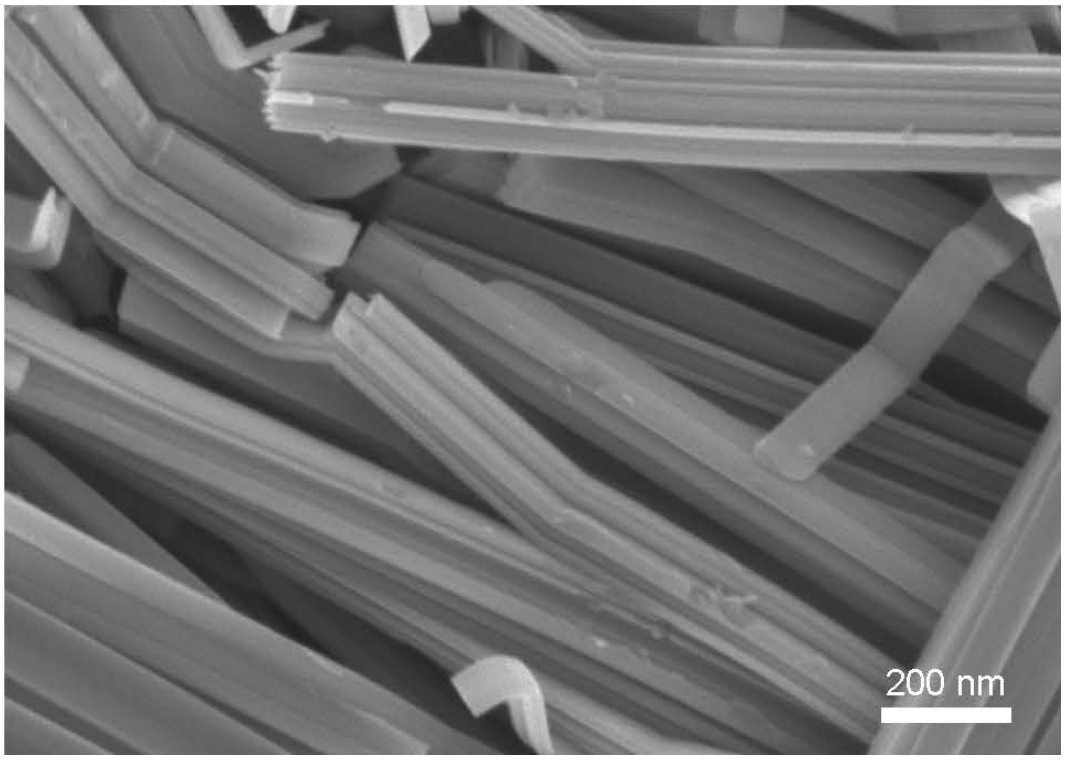

Figure S4. FESEM of the as-prepared H-NVO.

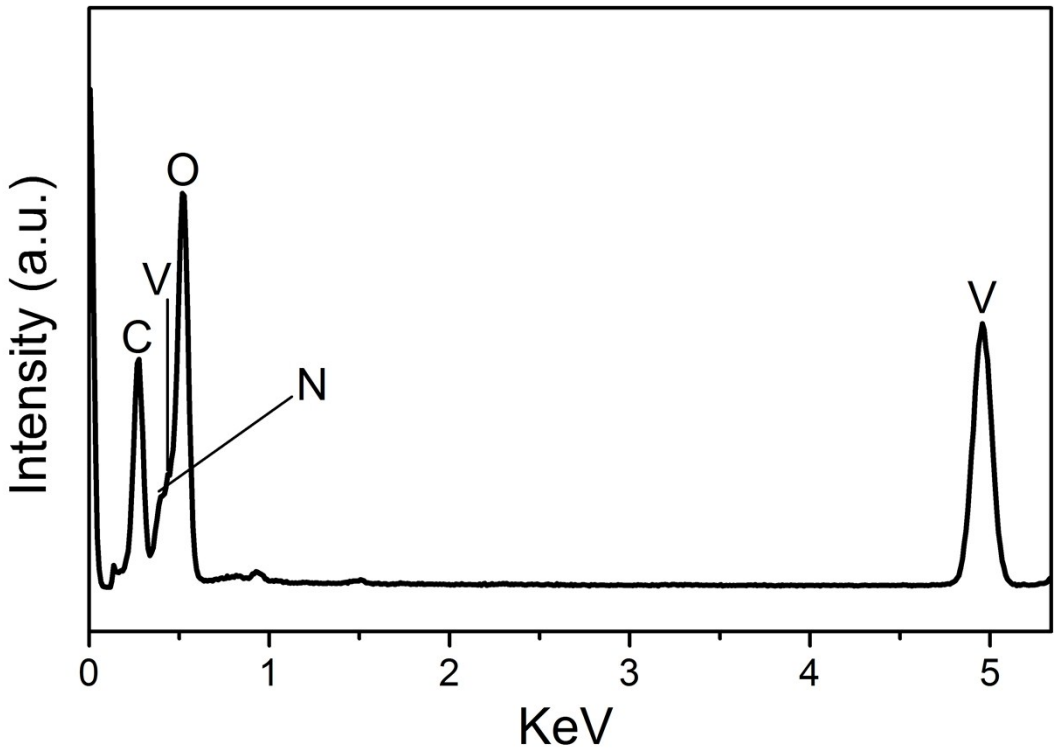

Figure S5. EDX spectrum of the as-fabricated H-NVO nanobelts.

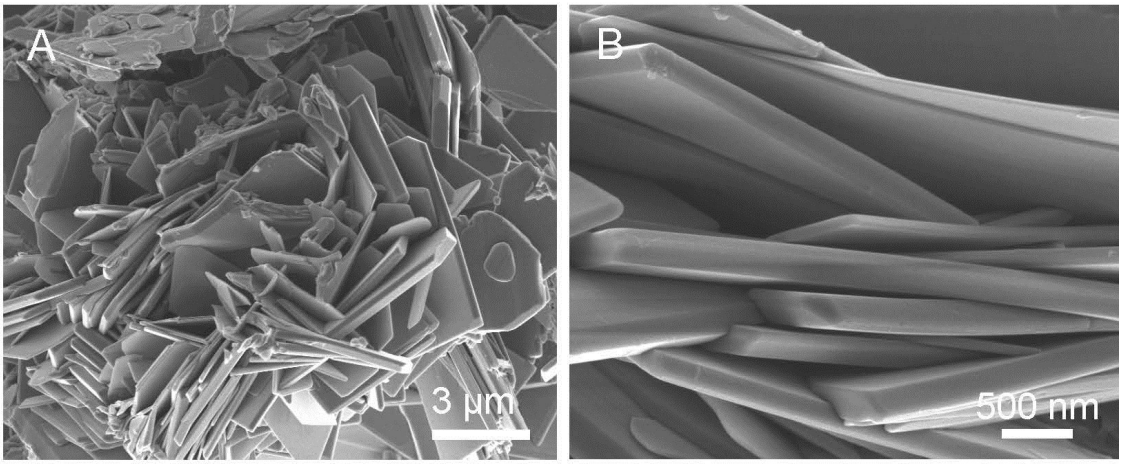

Figure S6. FESEM images of the as-prepared NVO. (A) low-magnification. (B) high-magnification.

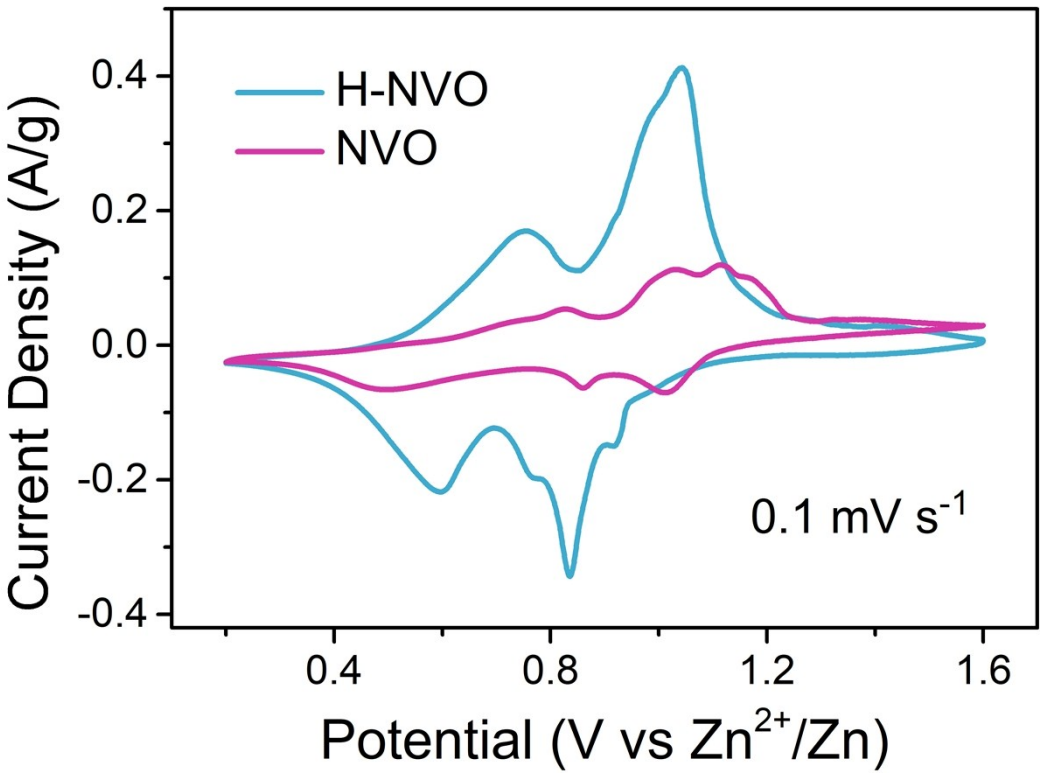

Figure S7. CV curves of the third cycle for H-NVO and NVO at the scan rate of 0.1 mV s^{-1}.

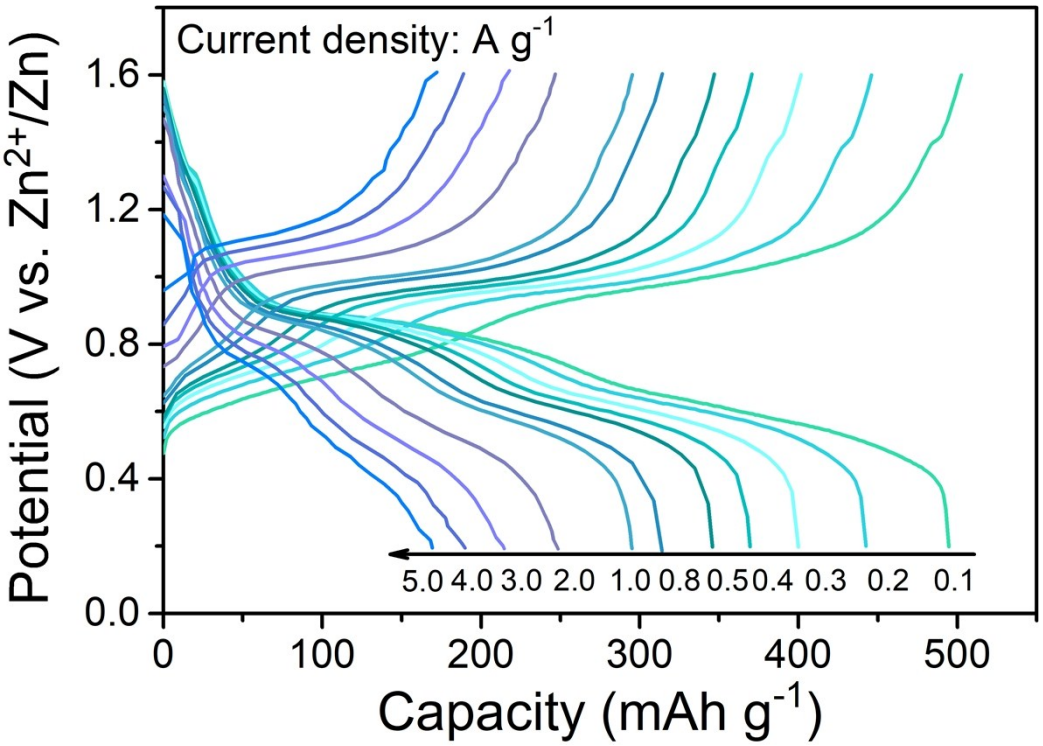

Figure S8. Representative galvanostatic charge/discharge curves at various current rates of the H-NVO electrode.

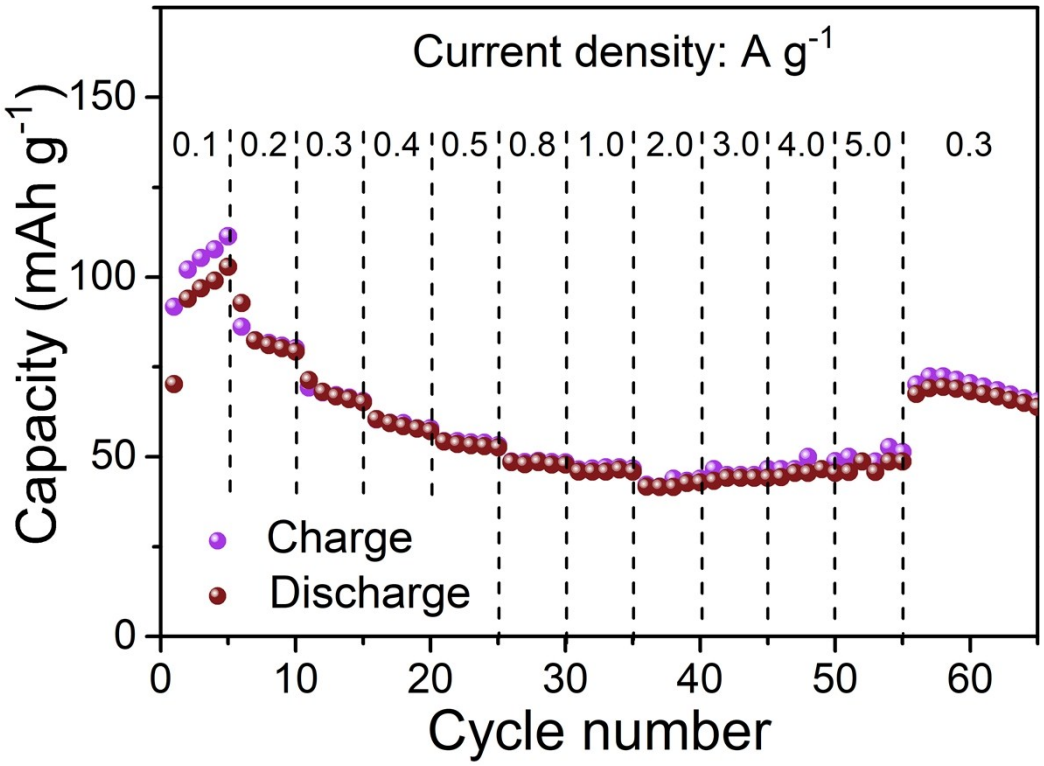

Figure S9. Rate capability at various current rates of the NVO electrode.

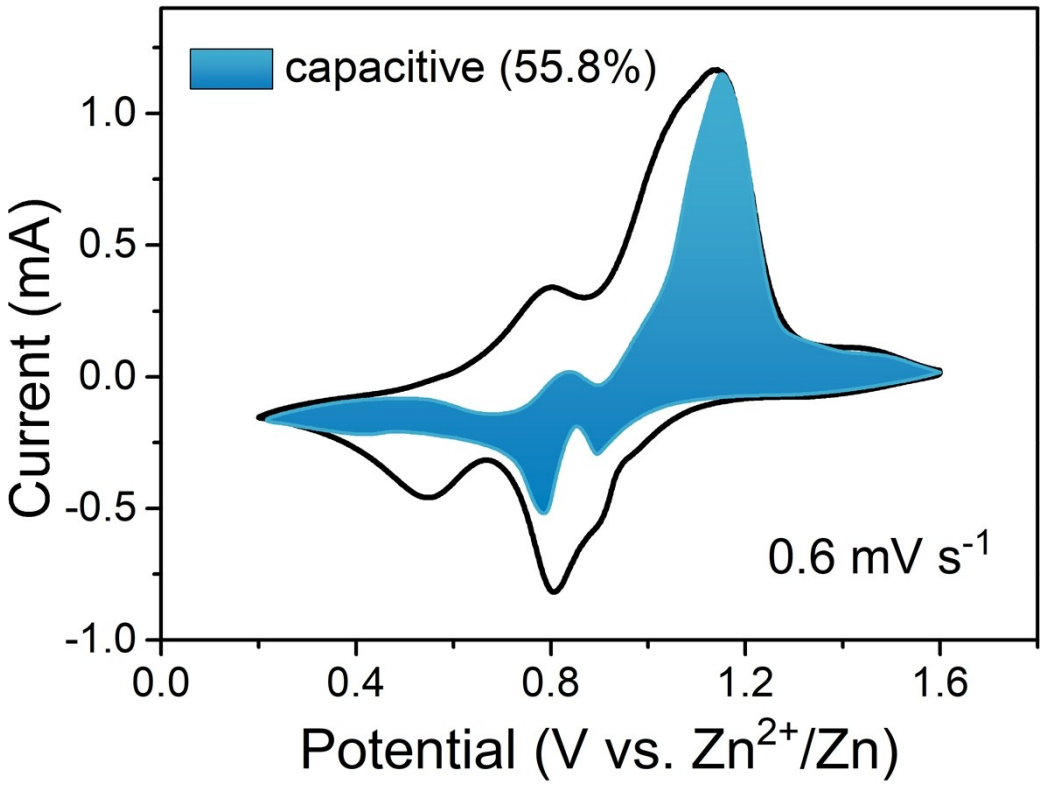

Figure S10. The contribution of capacitive charge storage as a function of the potential at the scan rate of 0.6 mV s^{-1} calculated based on the k_1 analysis.

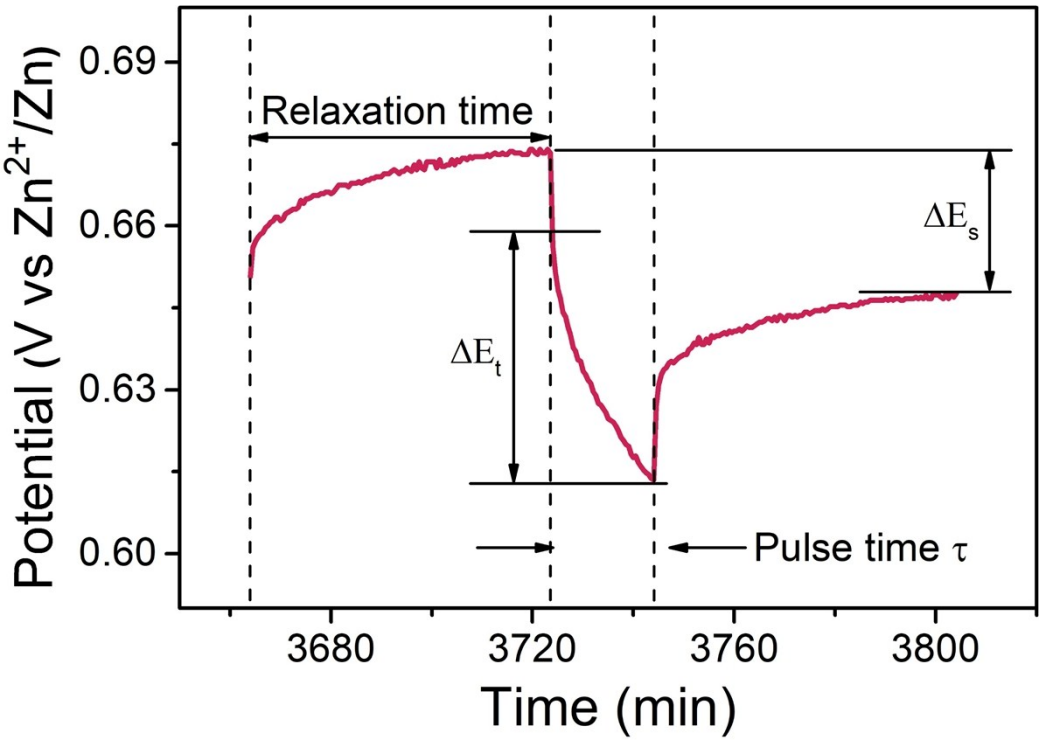

Figure S11. Schematic illustration of a signal step of the GITT measurement. The Zn^{2+} solid-state diffusion coefficient was obtained through the Galvanostatic Intermittent Titration Technique (GITT) measurement based on the following equation:

$$D_{Zn^{2+}}^{GITT} = \frac{4}{\pi\tau}\left(\frac{n_M V_M}{S}\right)^2\left(\frac{\Delta E_S}{\Delta E_t}\right)^2$$

Where τ is the constant current pulse time (s); n_M and V_M are the moles (mol) and molar volume (cm^3 mol^{-1}) of active material, respectively; S is the electrode/electrolyte contact area (cm^2); ΔE_s is the change in the steady-state voltage during a single step GITT experiment; ΔE_t is the change in a total cell voltage after the application of a constant current pulse during a single step GITT experiment. In our GITT measurement, a cell was charged or discharged at the current density of 50 mAh g^{-1} for 20 min, followed by a 1 h open circuit step to allow relaxation back to equilibrium.

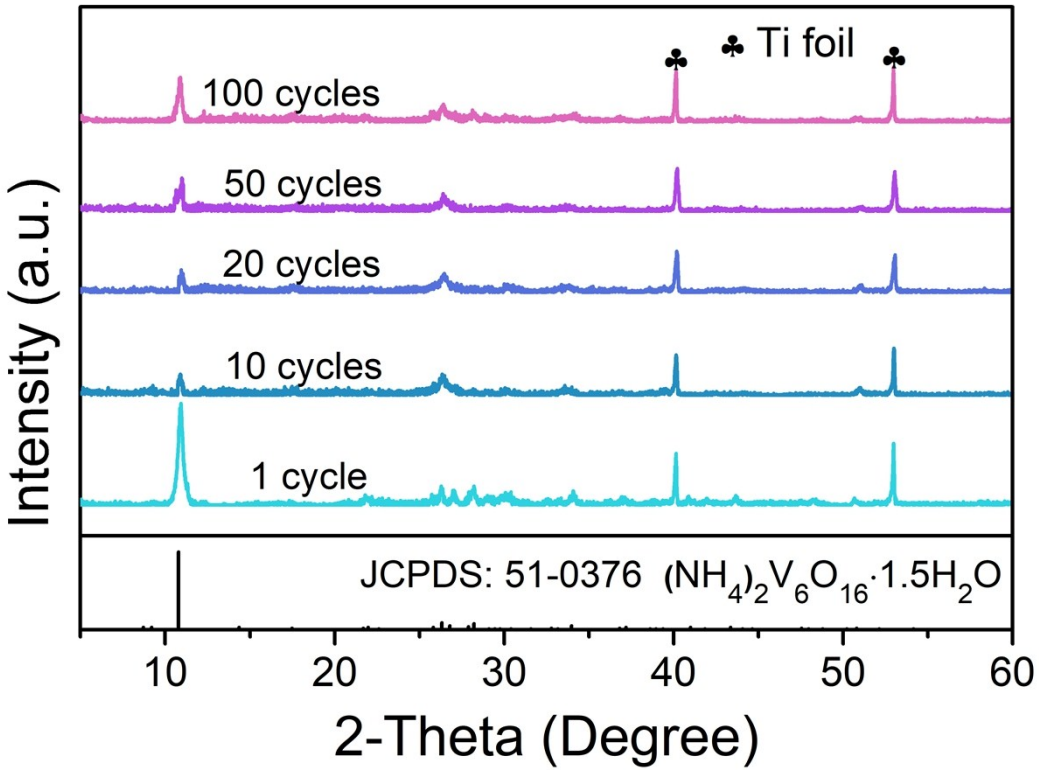

Figure S12. XRD patterns of the H-NVO electrode after 1st, 10th, 20th, 50th, and 100th cycles, respectively.

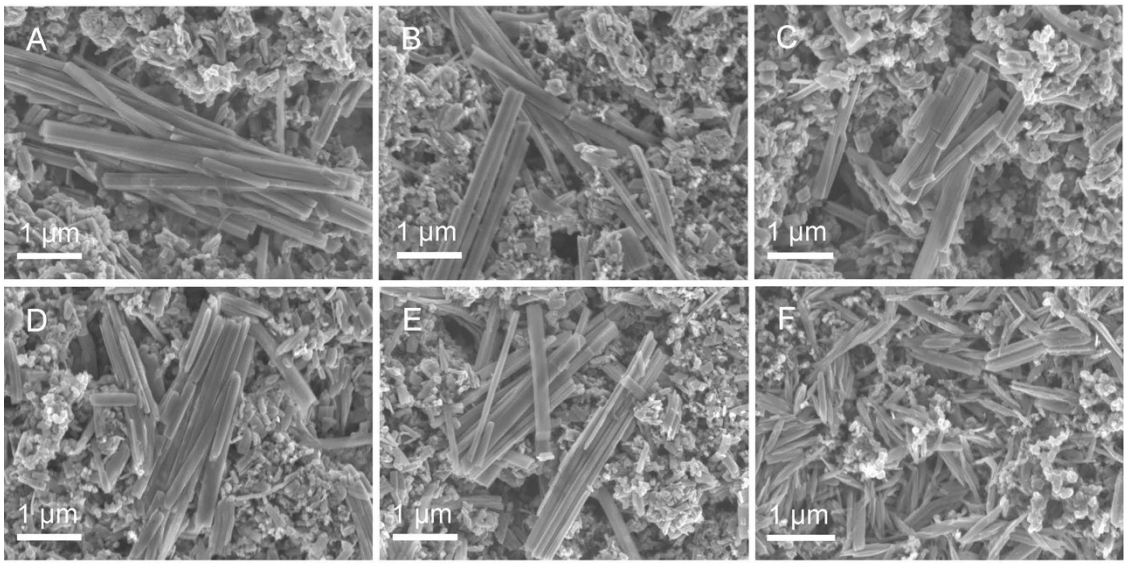

Figure S13. FESEM images of the H-NVO electrode after 1st (a), 10th (b), 20th (c), 50th (d), 100th (e) and 3000th (f) cycles, respectively.

Table S1. Comparison of the electrochemical performances over previous reported cathode materials in aqueous zinc ion batteries.

Cathode materials	Electrochemical performance	Reference
$(NH_4)_2V_6O_{16}\cdot 1.5H_2O$	152 mAh g^{-1} at 5 A g^{-1} (3000 cycles)	This work
$Na_{0.33}V_2O_5$	218.4 mAh g^{-1} at 1 A g^{-1} (1000 cycles)	[1]
$Mg_{0.34}V_2O_5\cdot 0.84H_2O$	ca. 88 mAh g^{-1} at 5 A g^{-1} (2000 cycles)	[2]
$Zn_3V_2O_7(OH)_2\cdot 2H_2O$	101 mAh g^{-1} at 0.2 A g^{-1} (300 cycles)	[3]
$H_2V_3O_8$	136.1 mAh g^{-1} at 5 A g^{-1} (1000 cycles)	[4]
$NaV_3O_8\cdot 1.5H_2O$	ca. 130 mAh g^{-1} at 4 A g^{-1} (1000 cycles)	[5]
LiV_3O_8	172 mAh g^{-1} at 0.133 A g^{-1} (65 cycles)	[6]
$Na_{1.1}V_3O_{7.9}$@rGO	171 mAh g^{-1} at 0.3 A g^{-1} (100 cycles)	[7]
$K_2V_8O_{21}$	ca. 125 mAh g^{-1} at 6 A g^{-1} (300 cycles)	[8]
α-$Zn_2V_2O_7$	138 mAh g^{-1} at 4 A g^{-1} (1000 cycles)	[9]
$Fe_5V_{15}O_{39}(OH)_9\cdot 9H_2O$	ca. 100 mAh g^{-1} at 5 A g^{-1} (300 cycles)	[10]
$Na_3V_2(PO_4)_3$	72 mAh g^{-1} at 0.05 A g^{-1} (100 cycles)	[11]
VO_2	ca. 75 mAh g^{-1} at 3 A g^{-1} (5000 cycles)	[12]
α-MnO_2	ca. 92 mAh g^{-1} at 1.54 A g^{-1} (5000 cycles)	[13]
β-MnO_2	135 mAh g^{-1} at 2 A g^{-1} (2000 cycles)	[14]
$ZnMn_2O_4$	ca. 80 mAh g^{-1} at 0.5 A g^{-1} (500 cycles)	[15]
$K_{0.8}Mn_8O_{16}$	ca. 150 mAh g^{-1} at 1 A g^{-1} (1000 cycles)	[16]
α-Mn_2O_3	82.2 mAh g^{-1} at 2 A g^{-1} (1000 cycles)	[17]
Mn_3O_4	106.1 mAh g^{-1} at 0.5 A g^{-1} (300 cycles)	[18]
MnO_x@N-C	100 mAh g^{-1} at 2 A g^{-1} (1600 cycles)	[19]
VS_2	110.9 mAh g^{-1} at 0.5 A g^{-1} (200 cycles)	[20]
MoS_2	88.6 mAh g^{-1} at 1 A g^{-1} (1000 cycles)	[21]
$Zn_3[Fe(CN)_6]_2$	ca. 80 mAh g^{-1} at 0.3 A g^{-1} (100 cycles)	[22]
ZnHCF@MnO_2	80 mAh g^{-1} at 0.5 A g^{-1} (1000 cycles)	[23]

References

1. P. He, G. B. Zhang, X. B. Liao, M. Y. Yan, X. Xu, Q. Y. An, J. Liu and L. Q. Mai, *Adv. Energy Mater.*, 2018, **8**, 1702463.
2. F. W. Ming, H. F. Liang, Y. J. Lei, S. Kandambeth, M. Eddaoudi and H. N. Alshareef, *ACS Energy Lett.*, 2018, **3**, 2602-2609.
3. C. Xia, J. Guo, Y. J. Lei, H. F. Liang, C. Zhao and H. N. Alshareef, *Adv. Mater.*, 2018, **30**, 1705580.
4. P. He, Y. L. Quan, X. Xu, M. Y. Yan, W. Yang, Q. Y. An, L. He and L. Q. Mai, *Small*, 2017, **13**, 1702551.
5. F. Wan, L. L. Zhang, X. Dai, X. Y. Wang, Z. Q. Niu and J. Chen, *Nat. Commun.*, 2018, **9**, 1656.
6. M. H. Alfaruqi, V. Mathew, J. J. Song, S. J. Kim, S. Islam, D. T. Pham, J. Jo, S. Kim, J. P. Baboo, Z. L. Xiu, K. S. Lee, Y. K. Sun and J. Kim, *Chem. Mater.*, 2017, **29**, 1684-1694.
7. Y. S. Cai, F. Liu, Z. G. Luo, G. Z. Fang, J. Zhou, A. Q. Pan and S. Q. Liang, *Energy Storage Mater.* 2018, **13**, 168-174.
8. B. Y. Tang, G. Z. Fang, J. Zhou, L. B. Wang, Y. P. Lei, C. Wang, T. Q. Lin, Y. Tang and S. Q. Liang, *Nano Energy*, 2018, **51**, 579-587.
9. B. Sambandam, V. Soundharrajan, S. Kim, M.H. Alfaruqi, J. Jo, S. Kim, V. Mathew, Y.-k. Sun and J. Kim, J. Mater. Chem. A, 2018, 6, 3850-3856.
10. Z. Peng, Q. L. Wei, S. S. Tan, P. He, W. Luo, Q. Y. An, L. Q. Mai, Chem. Commun., 2018, 54, 4041-4044.
11. G. L. Li, Z. Yang, Y. Jiang, C. H. Jin, W. Huang, X. L. Ding and Y. H. Huang,

Nano Energy, 2016, **25**, 211-217.

12. L. N. Chen, Y. S. Ruan, G. B. Zhang, Q. L. Wei, Y. L. Jiang, T. F. Xiong, P. He, W. Yang, M. Y. Yan, Q. Y. An and L. Q. Mai, *Chem. Mater.*, 2019, **31**, 699-706.
13. H. L. Pan, Y. Y. Shao, P. F. Yan, Y. W. Cheng, K. S. Han, Z. M. Nie, C. M. Wang, J. H. Yang, X. L. Li, P. Bhattacharya, K. T. Mueller and J. Liu, *Nat. Energy*, 2016, **1**, 16039.
14. N. Zhang, F. Y. Cheng, J. X. Liu, L. B. Wang, X. H. Long, X. S. Liu, F. J. Li and J. Chen, *Nat. Commun.*, 2017, **8**, 405.
15. N. Zhang, F. Y. Cheng, Y. C. Liu, Q. Zhao, K. X. Lei, C. C. Chen, X. S. Liu and J. Chen, *J. Am. Chem. Soc.*, 2016, **138**, 12894-12901.
16. G. Z. Fang, C. Y. Zhu, M. H. Chen, J. Zhou, B. Y. Tang, X. X. Cao, X. S. Zheng, A. Q. Pan and S. Q. Liang, *Adv. Funct. Mater.*, 2019, **29**, 1808375.
17. B. Z. Jiang, C. J. Xu, C. L. Wu, L. B. Dong, J. Li and F. Y. Kang, Electrochim. Acta, 2017, 229, 422-428.
18. J. W. Hao, J. Mou, J. W. Zhang, L. B. Dong, W. H. Liu, C. J. Xu, F. Y. Kang, Electrochim. Acta, 2018, 259, 170-178.
19. Y. Q. Fu, Q. L. Wei, G. X. Zhang, X. M. Wang, J. H. Zhang, Y. F. Hu, D. N. Wang, L. Zuin, T. Zhou, Y. C. Wu and S. H. Sun, *Adv. Energy Mater.*, 2018, 1801445.
20. P. He, M. Y. Yan, G. B. Zhang, R. M. Sun, L. N. Chen, Q. Y. An and L. Q. Mai, Adv. Energy Mater., 2017, 7, 1601920.
21. W. W. Xu, C. L. Sun, K. N. Zhao, X. Cheng, S. Rawal, Y. Xu and Y. Wang, *Energy Storage Mater.* 2019, **16**, 527-534.

22. L. Y. Zhang, L. Chen, X. F. Zhou and Z. P. Liu, Adv. Energy Mater., 2015, 5, 1400930.
23. K. Lu, B. Song, Y. X. Zhang, H. Y. Ma and J. T. Zhang, J. Mater. Chem. A, 2017, 5, 23628-23633.